RSC Advances

ROYAL SOCIETY OF CHEMISTRY

www.rsc.org/advances

RSC Advances

ARTICLE

The potential cytotoxicity and mechanism of VO_2 thin films for intelligent thermochromic windows†

Huaijuan Zhou,‡[a, b] Jinhua Li,‡[a, b] Shanhu Bao,[a] Donghui Wang,[a, b] Xuanyong Liu,[a, *] and Ping Jin[a, c, *]

Received 00th January 20xx,
Accepted 00th January 20xx

DOI: 10.1039/x0xx00000x

www.rsc.org/

Thermochromic vanadium dioxide (VO_2) film holds great promise for intelligent windows owing to marvelous semiconductor-metal transition (SMT), an active response to external temperature stimuli and near-infrared irradiation. To date, however, its potential biological effect on human cells has not well been characterized. In this work, homogeneous high quality VO_2 films with different thicknesses (30, 80, 120 nm) were prepared on quartz glass substrate. Afterwards, for the first time, we demonstrate the time-dependent and dose-dependent cytotoxicity of VO_2 film to human cells. Speciation analysis by ^{51}V NMR spectra and surface zeta potentials revealed the formation of vanadate(+5) and ADPV, an analogue of ATP. On the basis of energy metabolism or bioenergetics, a plausible hypothesis, i.e., "ATP dyssynthesis", is proposed here to elucidate the potential toxicity mechanism of VO_2 nanomaterial via vanadate-phosphate antagonism including two steps: (i) vanadate speciation from VO_2 surface chemistry; (ii) vanadate disturbing ATP synthesis as phosphate analogue. ATP stores energy to carry out various life processes; once its synthesis is hindered, vital movement will be impaired. From the perspective of surface modification and bioactivation, some practicable methods are recommended to compensate the potential cytotoxicity of VO_2 material. We expect this work can stimulate scientific interest to search for more versatile material design strategies to balance the energy-saving efficiency and environmental safety of VO_2 intelligent window coatings.

1. Introduction

Nowadays, energy conservation has become a global trend for sustainable development achieved by increasing energy efficiency and reducing energy consumption.[1] From this perspective, more and more attention has been paid to the intelligent windows that own switchable light transmittance capability and hold great promise for daily applications.[2, 3] Particularly, intelligent thermochromic windows, which are based on thermochromism materials like VO_2 film, have attracted growing interest due to their active response to environmental temperature stimulus that makes a reversible structural change from infrared-transparent semiconductive state to infrared-reflective metallic state.[4-6] VO_2 undergoes a semiconductor-to-metal transition (SMT) at a critical temperature T_c (68°C for bulk VO_2),[7] which has attracted growing attention as a thermochromic material and holds great promise for applications in intelligent windows.[8, 9] Since the NIR light radiation carries a large amount of solar energy, nowadays, increasing efforts have been made to exploit the marvelous SMT property of VO_2 to intelligently control NIR radiation for energy-saving purpose.

By so far, to achieve the daily application of VO_2 film in intelligent windows, the main attention has focused on the optimization of preparation methods and enhancement of energy-saving efficiency. However, a metal oxide nanomaterial may hold toxic potential to human health and ecology environment.[10] With regard to nanomaterials, a question must be asked, that is, how those man-made nanostructures could potentially interact with or influence biological systems. Exposure to nanomaterials may cause toxicity to biological systems. Although toxicity data for widely used nanomaterials like TiO_2 are available,[11] but for those newly developed nanomaterials like graphene,[12] fullerene,[13] VO_2, very little is known on their biological actions and interactions with living cells.

In fact, exposure of vanadium compounds can produce toxicity to mammalian respiratory system,[14, 15] liver[16, 17] and also cause adverse physiological effects on various microbes.[18-20] Toxicity of vanadium depends upon its physicochemical states, especially upon the valence states and solubility.[21, 22] Vanadium possesses six oxidation states and the most commonly found in the nature are V(+3), V(+4), and V(+5). Vanadium toxicity increases as the oxidation state ascends. However, to our best knowledge, current reports mainly focused on the toxicity of V_2O_3 and V_2O_5 particles, and very few studies were reported on the toxicity of VO_2, let alone its film. In terms of thermochromic VO_2 film for intelligent window coating, its exposure to human bodies is inevitable in the processes of film production, daily application and refuse disposal.

Herein, homogeneous high quality VO_2 films were fabricated on quartz glass with the aim to study the potential toxicity of immobilized VO_2 nanomaterial to human intrahepatic biliary epithelial cells. Zeta potential and pH measurements were performed to analyze the surface chemistry of VO_2 film. ICP-OES was used to study the release behaviors of vanadium species. NMR

[a] State Key Laboratory of High Performance Ceramics and Superfine Microstructure, Shanghai Institute of Ceramics, Chinese Academy of Sciences, Shanghai 200050, China.
[b] University of Chinese Academy of Sciences, Beijing 100049, China.
[c] Materials Research Institute for Sustainable Development, National Institute of Advanced Industrial Science and Technology, Nagoya 463-8560, Japan.

† Electronic Supplementary Information (ESI) available: Additional experimental details and relevant analysis. See DOI: 10.1039/x0xx00000x

‡ These authors contributed equally to this work.

spectra were recorded to analyze the vanadium speciation. Meanwhile, alamarBlue assay, live/dead cell staining, SEM, ATP assay and protein assay were combined to evaluate the cytotoxicity.

2. Materials and methods

2.1 Fabrication of specimens

The high quality VO_2 films were prepared by means of magnetron sputtering apparatus (ULVAC Corp., Model ACS-4000-C4) and the deposition details can be found in Supporting Information. Since float glass contains some elements such as Na, K, Ca, Mg, etc., which may interfere in the research results, fused quartz (composed of Si and O elements) was used as the substrate for VO_2 film deposition. The film thickness was measured by F20 thin-film analyzer (FILMSTRICS corp.). VO_2 films with different thicknesses (including 30 nm, 80 nm, 120 nm) were obtained and denoted as MS-30, MS-80 and MS-120, respectively. The quartz glass acted as control group (MS-0).

2.2 Characterization of specimens

The film crystalline structure was studied by X-ray diffractometer (XRD, Rigaku Ultima IV) with Cu Kα radiation (λ=0.15406 nm) at voltage of 40 kV, current of 40 mA, glancing incidence angle of 1° and scanning rate of 2 °/min. The surface morphology was examined by field-emission scanning electron microscopy (FE-SEM, FEI Magellan 400, US). XPS characterization was carried out on the surfaces of films after soaking them in PBS for 2 weeks to analyze the chemical valence state of V element. The ^{51}V NMR measurements were performed on Agilent DD2 600 MHz spectrometer operating at 25 °C with the fixed testing frequency of 157.7 MHz. The ^{51}V NMR chemical shifts were relative to $VOCl_3$ solutions. The free induction decay (FID) signals were exponentially line broadened (20 Hz for ^{51}V) prior to Fourier transformation.

2.3. Zeta potential measurements

The surface zeta potentials of MS-0, MS-30, MS-80 and MS-120 samples were measured by SurPASS Electrokinetic Analyzer (EKA; Anton Paar GmbH, Graz, Austria) equipped with a special cell for membrane/film. Samples (size 20 mm × 10 mm × 1 mm) were fixed on holders with double-sided adhesive tape (**Scheme S1**). 0.9% NaCl electrolyte solution was used as medium and pH value was adjusted by adding HCl and NaOH solutions.

2.4. Vanadium release measurements

The release characteristic of vanadium ions from VO_2 films soaked in PBS was detected by inductively coupled plasma optical emission spectrometry (ICP-OES, Varian Liberty 150, US). The pH of PBS was adjusted to 6.8 and 7.4 by adding HCl solution. The samples were placed in sterile microcentrifuge tubes (15 ml), immersed in new medium of 10 ml, and accordingly incubated at 37 °C for 1, 4, 7 and 14 days in static condition. At the end of each incubation period, all the leachates were collected for detection and supplemented with fresh media for further incubation.

2.5. pH measurements.

To determine the pH changes of solution when soaking VO_2 films, samples MS-0, MS-30, MS-80 and MS-120 were immersed in 6 ml NaOH aqueous solution with an initial pH = 10.40 in sterile microcentrifuge tubes and accordingly incubated at 37 °C for 1, 2, 3, 4, 5, 6 and 7 days in static condition. After the incubation of each period, the pH was measured by pH meter (FE20–FiveEasy™, METTLER TOLEDO).

2.6. Cell proliferation and viability

Human intrahepatic biliary epithelial cells (HIBEpiC) were purchased from ScienCell (San Diego, California, US). Cell proliferation and viability were evaluated by AlamarBlue assay (AbD Serotec Ltd., UK). Cells were seeded on samples with density of 5 × 10^4 cells/well and five samples per group were tested for each culture period (1, 4 and 7 days). After each period, the culture medium was removed and 500 µl fresh medium with 10% AlamarBlue was added to each well, followed by another incubation of 4 h. Cell proliferation and viability were calculated according to the manufacturer's instruction.

2.7. Live/dead cell staining

Live/Dead Cell Staining Kit (BioVision, US) was used following the manufacturer's instruction. Briefly, cells were seeded on samples (5 × 10^4 cells/well) and cultured for 4 days. Red fluorescent dye, propidium iodide (PI), and green fluorescent dye, calcein-AM were used to stain dead and live cells with final concentrations of 5 µM and 2 µM in PBS, respectively. Gently washed in PBS thrice, 100 µl of mixed solution was added to each well, then incubated at 37 °C for 15 min. A confocal laser scanning microscopy (CLSM, Leica SP8, Germany) was used to visualize the live and dead cells.

2.8. Cell morphology observation

SEM was utilized to further investigate cell morphology and cell-material interactions. After each culture period, the samples were transferred to a new 24-well plate and rinsed gently with PBS thrice and then fixed with 2.5% glutaraldehyde solution for overnight. Prior to SEM observation, the samples were dehydrated in a series of ethanol solutions (30, 50, 75, 90, 95, and 100 v/v%) for 10 min each sequentially, along with the final dehydration conducted in absolute ethanol (twice) followed by drying in hexamethyldisilizane/ethanol solution series.

2.9. Intracellular ATP level

The ATP level inside cells was measured by the luciferin-luciferase method following the protocol of ATP assay kit (Beyotime, China). HIBEpiC were seeded on samples MS-0, MS-30, MS-80 and MS-120 in 24-well plate (1 × 10^5 cells/well). Five samples were used for each group. After culture of 4 days, cells were washed twice with PBS and then resolved in ATP lysis buffer on ice. ATP in cell lysate was measured using Synergy H4 Hybrid Microplate Reader (BioTek, US), and the ATP concentration was normalized to the standard curve. Protein contents were measured using BCA Protein Assay kit (Beyotime, China) to correct the different samples for comparison of ATP concentration.

2.10. Statistical analysis

Statistically significant differences (P) between various groups were measured using one-way analysis of variance and Tukey's multiple comparison tests on a GraphPad Prism 5 statistical software package. All the data were expressed as means ± standard deviation (SD). A value of $P < 0.05$ was considered to be statistically significant and denoted as "*", $P < 0.01$ was "**", and $P < 0.001$ was "***".

3. Results and discussion

3.1. Sample characterization

Figure 1a-c reveals thickness-dependent morphology of VO_2 films on quartz, with homogeneous compact nanostructures. One can distinguish clear size polydispersity in addition to the stochastic shape of VO_2 crystallites. The nanoparticles were worm-like for MS-30 and became much larger for MS-80. For MS-120, however, the particles turned out to be cobblestone-like structures of uneven size. That increasing deposition time produced particle size growing was attributed to the Volmer-Weber growth mode of VO_2 nanofilms. XRD ϑ-2ϑ scan profiles were measured on as-deposited films at ambient temperature, as shown in **Figure 1**d. Only XRD peaks corresponding to the signal of monoclinic VO_2 phase were observed. All the positions of peaks were concordant with the standard reference data

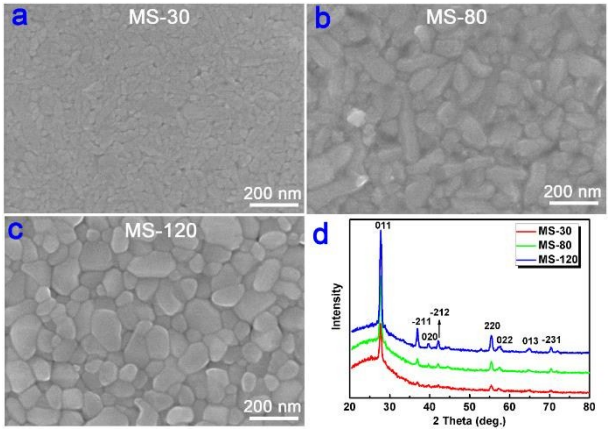

Figure 1. (a~c) FE-SEM images and (d) Grazing incident XRD patterns of the various VO_2 films with different thicknesses (30 nm for sample MS-30, 80 nm for sample MS-80, 120 nm for sample MS-120).

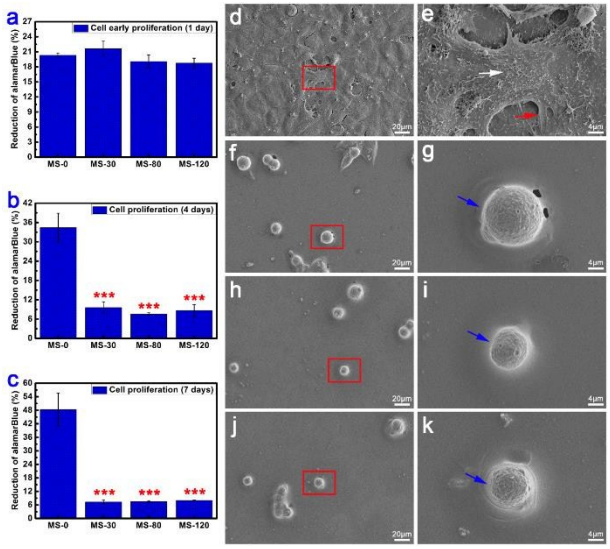

Figure 2. (a~c) Proliferation results of HIBEpiC after culture of 1, 4 and 7 days on samples MS-0, MS-30, MS-80 and MS-120, accompanied by the SEM morphology of HIBEpiC after culture of 4 days on surfaces of MS-0 (d, e), MS-30 (f, g), MS-80 (h, i) and MS-120 (j, k). Note: white arrow, showing the extracellular matrix mineralization; red arrow, showing the lamellipodia and filopodia extensions; blue arrow, showing the hardly seen lamellipodia/filopodia.

(JCPDS No. 72-0514), indicating the exclusive formation of single-phase VO_2 polycrystalline films. The raise of VO_2 film thickness brought about the much stronger diffraction peaks, accounting for better crystallinity. Besides, the value of full width at half maxima (FWHM) of the predominant orientation (011) was declined with the increment of film thickness. According to Scherrer formula, the average grain size of the films had a positive correlation with the reciprocal of FWHM, which provided another evidence for the growing particle size. Herein, we also demonstrate that the SMT property and energy-saving efficiency of VO_2 film can be tailored and optimized in a film thickness dependent manner (**Figure S1**).

3.2. Cytotoxicity of VO_2 nanofilm

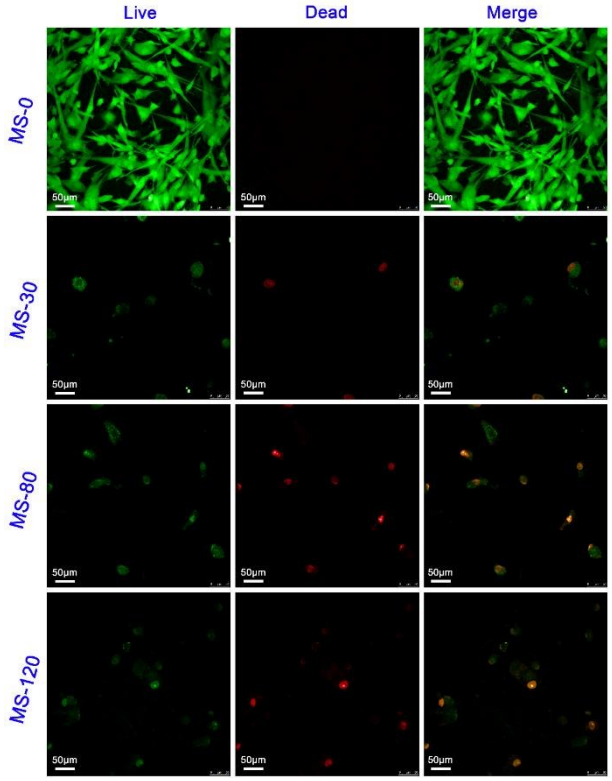

Figure 3. Live/dead staining results of HIBEpiC viability after culture of 4 days on surfaces of samples MS-0, MS-30, MS-80 and MS-120 that were observed on a confocal laser scanning microscopy (CLSM). Note: green color for live cells, red color for dead cells.

Figure 2 shows the proliferation and morphology of HIBEpiC cultured on various samples. At early culture of 1 day, HIBEpiC can well adhere on the VO_2 films, showing no significant difference between VO_2 and control (**Figure 2**a). However, after culturing for 4 days, HIBEpiC proliferation was sharply inhibited on VO_2 films, while they can maintain a steady growth on control (**Figure 2**b), indicating that the presence of VO_2 film on quartz glass caused severe cytotoxicity toward HIBEpiC. Prolonging the culture to 7 days, as shown in **Figure 2**c, the growth retardation of HIBEpiC continued and implied the ongoing cell death. SEM was used to analyze the cell morphology development and cell-material interaction of HIBEpiC cultured on various surfaces for 4 days. As seen in **Figure 2**d, the surface of quartz glass was thoroughly covered by the HIBEpiC and the cells connected well with each other. On the contrary, markedly reduced cells were observed on the VO_2 films and most of them still maintained a spherical or spindle morphology (**Figure 2**f, h, j). Therefore, the cell morphology was quite consistent with the proliferation trend. At high magnification, the HIBEpiC on quartz glass spread well, exhibiting a multipolar spindle morphology (**Figure 2**e). Focusing on the cell membrane, as indicated by the white arrow, visible particulate matter was prevalent, showing the exuberant extracellular matrix mineralization (ECM). Moreover, abundant lamellipodia and filopodia extensions were found (red arrow), indicating the pervasive intercellular communications and cell-materials interactions. With regard to VO_2 films, however, spherical cell morphology, and hardly seen lamellipodia/filopodia (indicated by blue arrow in **Figure 2**g, i, k) revealed the poor cell viability and stagnant cell fate toward cell death. To visualize and distinguish between live and dead cells, live/dead cell staining was further

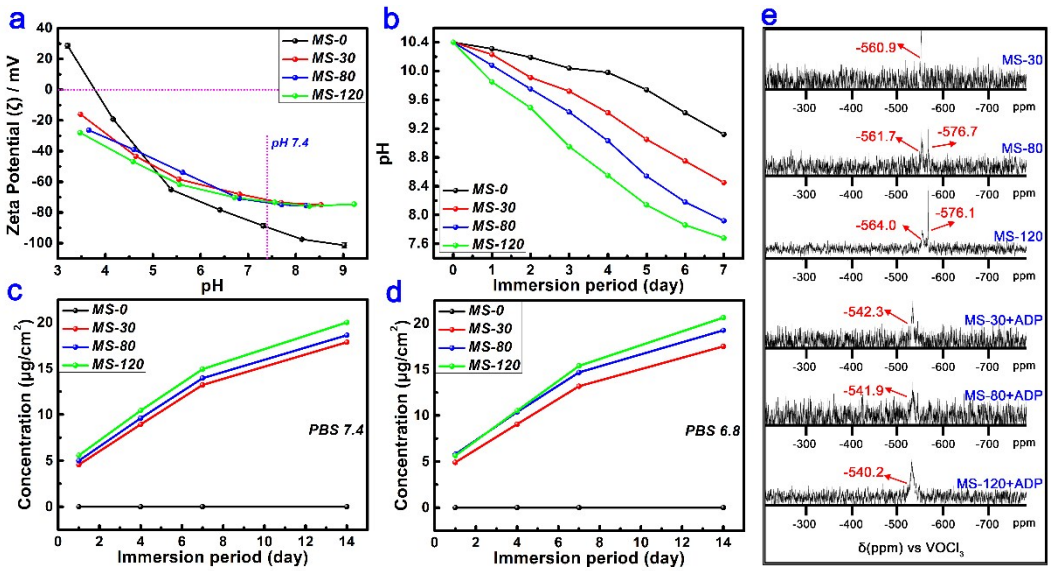

Figure 4. (a) Results of surface zeta potentials (ζ) of samples MS-0, MS-30, MS-80 and MS-120. (b) Changes of pH values when immersing MS-0, MS-30, MS-80 and MS-120 in PBS with initial pH=7.40. (c~d) Release features of vanadium ions from MS-0, MS-30, MS-80 and MS-120 surfaces. (e) ^{51}V NMR spectra of various extraction solutions after immersing MS-30, MS-80 and MS-120 in PBS (pH=7.40) for 14 days, accompanied by the corresponding ^{51}V NMR spectra of the above extraction solutions with adding of ADP (50 mM).

performed and the results were given in **Figure 3** (green for live cells, red for dead cells). Nearly no dead cells were observed under the CLSM and the HIBEpiC grew well on MS-0. However, prevailing cell death were present on VO_2 films and even some dying cells were alsoobserved. Overall, the live/dead staining results were quite consistent with the cell proliferation and SEM results. Considering the presence of VO_2, it is inferred that the observed cytotoxicity may be caused by the toxic vanadium element.

3.3. Plausible cytotoxicity mechanism.

In fact, vanadium toxicity has been of a great concern although it is one of the essential trace elements in human body,[23] and so, substantial efforts have been made to clarify the mechanisms of vanadium metabolism and toxicology.[24-26] To figure out the reason for observed cytotoxicity, it is quite essential here to analyze the surface aqueous chemistry of vanadium dioxide and speciation of vanadium element. The surface zeta potentials *versus* pH for each group are shown in **Figure 4**a and all the curves exhibit descending trends with the ascending pH. It is well known that a strong electric field exists at an aqueous solution/oxide interface.[27] This interfacial electric field is produced by the surface charge of oxide, which can interact with the dipole moment of water molecules and induce ordering of up to several layers at the interface.[28, 29] The strength and direction of the electric field at an aqueous solution/oxide interface are a function of the pH of solution and the IEPS of substrate. The IEPS, namely, isoelectric point of surface, is the pH value of the aqueous solution in which the total surface charge density is zero. The surface of a substrate is negatively (positively) charged when the pH of the solution is greater (less) than the IEPS of the substrate.[30-33] According to **Figure 4**a, all the surfaces of VO_2 films were negatively charged since the present pH range was above the IEPS of VO_2. At prevalent oxic conditions near neutral to slightly alkaline pH, soluble vanadate(+5) anion, i.e., $H_2VO_4^-$, is the predominant specie, in which the pentavalent oxidation state is the most stable form among its various oxidation states.[23, 34] Therefore, an initial chemical redox reaction might occur at the VO_2/solution interface:

$$4VO_2 + 4OH^- + O_2 + 2H_2O = 4H_2VO_4^- \quad (1)$$

To support this, the pK_a values for vanadate were given below:[35]

$$H_3VO_4 + H_2O \leftrightarrow H_2VO_4^- + H_3O^+ \text{, p}K_a\text{=3.5} \quad (2)$$

$$H_2VO_4^- + H_2O \leftrightarrow HVO_4^{2-} + H_3O^+ \text{, p}K_a\text{=7.8} \quad (3)$$

$$HVO_4^{2-} + OH^- \leftrightarrow VO_4^{3-} + H_2O \text{, p}K_a\text{=12.5} \quad (4)$$

From the above, $H_2VO_4^-$ formation is reasonable in the present experimental conditions and negatively charged surface can be formed on VO_2 in a wide pH range. In fact, only by dissolving in non-oxidizing strong acids can VO_2 produce the vanadyl cations (VO^{2+}) with positively charged surface ($VO_2+2H^+=VO^{2+}+H_2O$).[36] Meanwhile, the surface zeta potentials from various VO_2 films showed a thickness-dependent difference (**Figure 4**a) that is quite reasonable. This difference showed to diminish gradually with pH increase, especially at pH=7.4, indicating a chemical equilibrium was established in these aqueous systems. In reality, at the physiological pH and ionic strength, vanadate(+5) is almost exclusively present in the $H_2VO_4^-$ form.[23] Besides, for quartz substrate (MS-0), a hydration process occurred at the IEPS of ~3.7 ($SiO_2+H_2O=H_2SiO_3$).[37, 38] At the IEPS, the total charge density of the hydrated surface on quartz was zero. Upon departure from the IEPS, the corresponding chemical reactions occur at the solution/quartz interface ($H_2SiO_3+OH^- \rightarrow HSiO_3^- +H_2O$, > IEPS; $H_2SiO_3+H^+ \rightarrow H_3SiO_3^+$, < IEPS). It should be noted that MS-0 had a significantly different characteristic of surface zeta potential from that of VO_2 films.

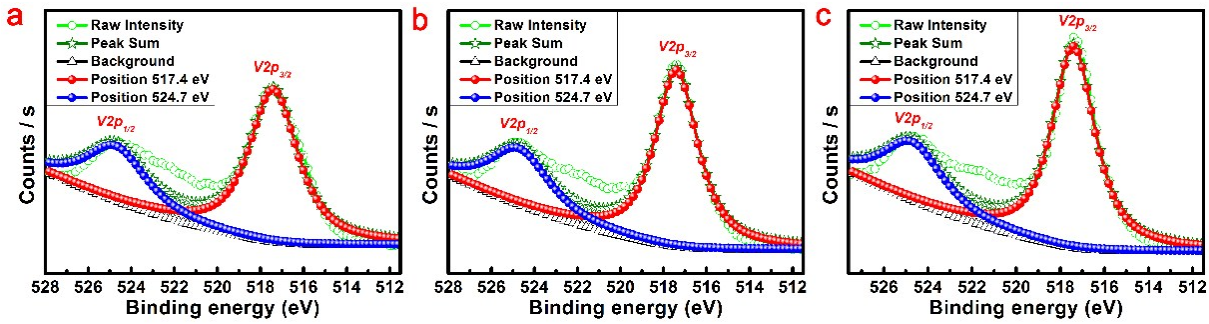

Figure 5. XPS analysis results on the surfaces of VO_2 films ((a) for MS-30, (b) for MS-80, (c) for MS-120) after immersing them in PBS for 2 weeks.

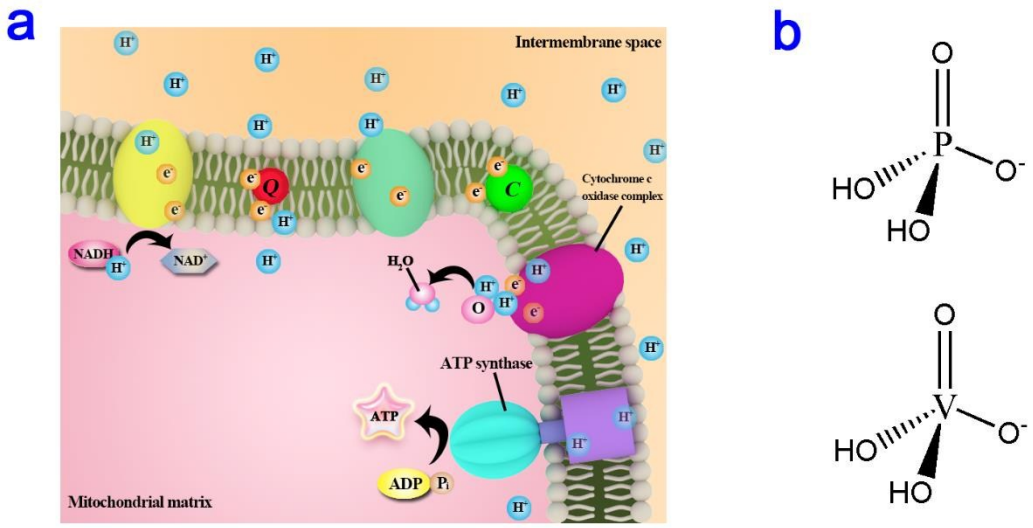

Figure 6. (a) Electron transport chain in the inner mitochondrial membrane. A sequence of electron carrier molecules (membrane proteins) shuttle electrons down a series of redox reactions that release energy used to produce ATP. (b) Schematic geometrical construction o inorganic phosphate and vanadate ions.

Furthermore, continuous pH measurements were conducted on NaOH aqueous solutions (initial pH = 10.40) for samples immersion within 7 days. It can be seen from **Figure 4**b that, for MS-0 sample, namely, quartz, the pH of solution gradually dropped from 10.40 to 9.12 within the 7 days of immersion in a slow manner. In comparison, all the VO_2 films samples suffered from an evident drop of solution's pH throughout the immersion period; the pH decreased from 10.40 to 8.45, 7.92 and 7.68 for MS-30, MS-80 and MS-120, respectively. As can be seen in **Figure 4**b, an obvious gap existed between the VO_2 samples and the quartz. On the basis of the results, it was deliberately concluded that the significant pH change was caused by the OH^- depletion.[39, 40] Therefore, the pH changes had an accordant correlation with the surface zeta potentials in **Figure 4**a. Specially, equation (1) depleted OH^- ions to lower the pH and produced $H_2VO_4^-$ to form a negatively charged surface at physiological pH. It is also worth mentioning that each pH measurement can refresh the air in the sealed microcentrifuge tubes to supply dissolved oxygen at the same time, which was essential for the formation of $H_2VO_4^-$ since its formation depleted O_2 molecules as equation (1). In fact, the oxygen supply is also essential for cell culture. The release feature of vanadium ions from VO_2 films was shown in **Figure 4**c-d. From this figure, the vanadium ions were released from VO_2 films in a time-dependent manner. To demonstrate this, ^{51}V NMR spectra were measured on extraction solution of VO_2 films in PBS, as shown in **Figure 4**e. The chemical shift (δ) at around -560 ppm corresponded to mononuclear tetrahedral vanadate (T_1). The appearance of δ at about -580 ppm belonged to the divanadate (T_2).[41-43] The transformation of T_1 to T_2 can be expressed as follow:[44, 45]

$$2T_1 \leftrightarrow T_2, [T_2] = K_1[T_1]^2 \quad (5)$$

To further demonstrate the formation of V(+5), XPS technique was used to investigate the chemical valence of surface V atoms. The results are shown in **Figure 5**. For pure VO_2 phase, the peaks assigned to $V2p_{1/2}$ and $V2p_{3/2}$ are located at 523.5 eV and 516.3 eV, respectively.[6] After immersing the VO_2 films in PBS for 2 weeks, their surfaces were gradually oxidized to be the pentavalent (+5) forms, evidenced by the $V2p_{1/2}$ peak at 524.7 eV and $V2p_{3/2}$ peak at 517.4 eV, which belong to the characteristic peaks of V2p in V_2O_5 phase.[46]

In biological systems, +5 valent $H_2VO_4^-$ is the most comm intracellular form and can be actively transported into cells.[47-50] Since among subcellular organelle, mitochondria has been proposed as an important target for vanadium accumulation and toxicity,[34, 51, 52] we thus hypothesize that the observed cytotoxicity to HIBEpiC w caused by the vanadate(+5) uptake into cells and accumulation in mitochondria, affecting the normal functions of mitochondria. Mitochondria, the powerhouse of the cell, produce most of the cellular energy supply of ATP to support various vital movemer s

Table 1. Some equilibrium constants for the vanadate/AMP, vanadate/phosphate systems at a physiological pH.

Species	Equilibrium constant	Reference
AMPV	9.2 M^{-1}	44
$AMPV_2$	12 M^{-1}	44
V_i-P_i anhydride	11.7 M^{-1}	68

Note: AMP, adenosine 5'-monophosphate; AMPV, adenosine 5'-monophosphate vanadate; $AMPV_2$, adenosine 5'-monophosphate divanadate; V_i-P_i anhydride, vanadate-phosphate anhydride

including cell spreading, growth and differentiation, etc.[53, 54] ATP synthesis from ADP and phosphate (P_i) is catalyzed by ATP synthase (*ADP*+P_i → *ATP*) as illustrated in **Figure 6**a. With regard to the phosphate(+5) group, its protonation reactions in aqueous solution are given below:[35]

$$H_3PO_4 + H_2O \leftrightarrow H_2PO_4^- + H_3O^+, \text{ p}K_a=2.1 \quad (6)$$

$$H_2PO_4^- + H_2O \leftrightarrow HPO_4^{2-} + H_3O^+, \text{ p}K_a=7.2 \quad (7)$$

$$HPO_4^{2-} + OH^- \leftrightarrow PO_4^{3-} + H_2O, \text{ p}K_a=12.7 \quad (8)$$

From the similar pK_a values for vanadate and phosphate, it can be seen that an analogy may exist in their electronic properties. On the other hand, according to the structure parameters of inorganic vanadate and phosphate: r(O^{2-})=1.36Å, d(V-O)=1.72Å, d(P-O)=1.54Å; V-O and P-O distances of four-coordination tetrahedral geometry where r(V^{+5})=0.36Å and r(P^{+5})=0.17Å, vanadate and phosphate are structural analogues since the geometrical diameters are 6.2Å and 5.8Å, and the volumes of circumscribing spheres are 125 $Å^3$ and 102 $Å^3$, respectively (**Figure 6**b).[55, 56] From a geometrical perspective, vanadate and phosphate are essentially indistinguishable, making vanadate an efficient competitor for phosphate in binding sites commonly targeted by phosphate. Thus, it is reasonable to infer that vanadate should behave as an analogue of phosphate in a biological system due to their electronic and structural analogy.[57, 58]

In view of the structural and electronic analogy between vanadate and phosphate, during ATP synthesis, the formation of phosphate anhydride and ester bonds may be antagonized by the occurrence of vanadate anhydride and ester bonds:[56, 59]

$$ROH + H_2VO_4^- \leftrightarrow ROVO_3H^- + H_2O \quad (9)$$

$$ROPO_3H^- + H_2VO_4^- \leftrightarrow ROP(O)_2OV(O)_2OH^{2-} + H_2O \quad (10)$$

The above reactions could produce vanadate ester and vanadate-phosphate anhydride as the analogues of phosphate ester and anhydride, which may cause adverse effects on ATP synthesis through the vanadate-phosphate antagonism. Some ATP analogues, such as ADPV, AMPV, AMV, have been previously reported to exist in the vanadate-adenosine/AMP/ADP/ATP system.[42, 44, 60] **Table 1** lists some equilibrium constants for vanadate-AMP and vanadate- phosphate systems at physiological pH. To verify that possibility of ADPV formation, ADP was added to the extraction solution of VO_2 in PBS, followed by ^{51}V NMR measurements, as shown in **Figure 4**e. The chemical shift δ at around -540 ppm was assigned to V_γ-P_β anhydride bond in ADPV, an analogue of ATP.[41-43] This coordination reaction is given below:[44, 45]

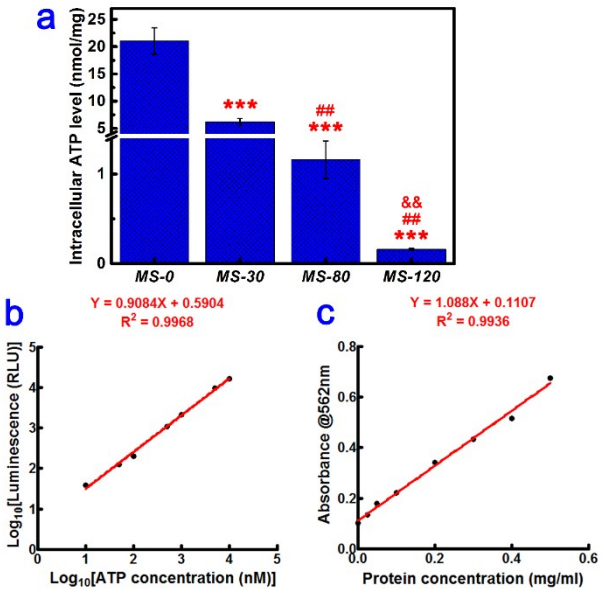

Figure 7. (a) Intracellular ATP levels of HIBEpiC after culture of 4 days on surfaces of MS-0, MS-30, MS-80 and MS-120 samples, accompanied by the corresponding standard curves of ATP concentration (b) and protein level (c). Notes: ***P < 0.001 *versus* MS-0; ##P < 0.01 *versus* MS-30; &&P < 0.01 *versus* MS-80.

$$T_1 + L \leftrightarrow TL, [TL] = K_2[T_1][L] \quad (11)$$

where *L* means the ligand ADP, *TL* is the product ADPV. According to equation (11), the formation of ADPV will decrease the concentration of mononuclear vanadate (T_1), which can make the chemical equilibrium of equation (5) shift left and thus reduce the concentration of divanadate (T_2). As a result, their resonance signals disappeared.

Since the ATP synthesis can be interrupted by vanadate, the level of ATP concentration inside a cell will reflect it accordingly. To verify that, intracellular ATP levels were determined on HIBEpiC, as shown in **Figure 7**. From the data, the ATP level inside an individual cell was sharply reduced after culturing HIBEpiC on VO_2 for 4 days. Meanwhile, combined with the corresponding proliferation results in **Figure 2**b, the interference of vanadate on ATP synthesis functioned in a dose-dependent manner. As a result, a cell cannot metabolize normally to produce ATP to support spreading and proliferation, and gradually dies out (**Figures 2-3**). To detoxify vanadate(+5), a cell will strain every nerve to bioreduce vanadate to vanadyl (VO^{2+}, +4), through reduced glutathione (GSH), flavoenzymes or nicotinamide adenine dinucleotide ($FADH_2$/NADH), nicotinamide adenine dinucleotide phosphate (NADPH), which causes inhibition of mitochondrial respiratory chain as side effect and seems to quench a thirst with poison.[34, 47, 60] In addition, other potential mechanisms of VO_2 material may also exist behind the observed cytotoxicity. On the one hand, the vanadyl (VO^{2+}) cation formed by bioreduction of vanadate anion has the potential to induce the production of reactive oxygen species (ROS) in a Fenton-like reaction, for instance, the formation of •OH hydroxyl radicals ($VO^{2+}+H_2O_2+H^+ \rightarrow VO^{3+}+H_2O+{}^{\bullet}OH$).[34, 61] On the other hand, the VO_2 material shows a semiconductor state at low temperature. The conduction band, valence band and band gap are -4.85 eV (E_c), -5.45 eV (E_v) and 0.6 eV (E_g), respectively.[6] As a result, the E_c value (-4.85 eV) is lower than

the cellular redox potential ranging from -4.12 eV to -4.84 eV.[62] Therefore, direct electron transfer may occur from biomolecular redox couples, which maintain the cellular redox potential and cellular homeostasis, to the conduction band of VO_2, thus causing oxidative stress induced cytotoxicity.[63-67]

Besides, on the basis of the Endosymbiotic theory, a bacterium is analogous to the mitochondrion of a mammalian cell. Therefore, the respiration is similar between bacterium and mitochondrion. As a result, it is reasonable to infer that VO_2 film can also exert potential toxic effect on bacteria just as it does to mitochondria, exhibiting antibacterial ability that would be beneficial for application in self-cleaning windows. In this context, further investigation work need to be done to explore the possible antimicrobial properties in future.

As a marvelous thermochromic nanomaterial, VO_2 holds great promise for applications in smart windows and nanodevices owing to its unique semiconductor-metal transition (SMT), an active response to external temperature stimuli and near-infrared irradiation. The present study pointed out the potential cytotoxicity of VO_2 nanofilm for the first time, and thus was expected to be able to stimulate wide scientific interest to search for more versatile material design strategies to enhance the environmental safety of thermochromic VO_2 material in the meantime of improving the energy-saving efficiency for smart window applications. From the perspective of surface coating and modification, some oxide materials, such as TiO_2, ZnO, etc, hold great promise for compensating the potential cytotoxicity of VO_2 film owing to their excellent bioactivity and biocompatibility. By depositing on VO_2 film to form spatial barrier, these oxide overlayers can exert their beneficial biological effects and inhibit VO_2 oxidation and vanadium release. This feasible surface coating strategy may also endow the composite film with other desired properties, such as enhanced antireflective and self-cleaning functions contributed by their optical effect and photocatalytic activity, which is extremely attractive for intelligent thermochromic windows.

4. Conclusions

In this study, homogeneous thermochromic VO_2 nanofilms with high quality (30 nm, 80 nm, 120 nm in thickness) were successfully deposited on quartz glass by reactive magnetron sputtering method. Subsequently, the potential cytotoxicity of VO_2 nanofilm to human cells was demonstrated for the first time in a time-dependent and dose-dependent manner. Surface chemistry and speciation analysis results confirmed the formation of vanadate(+5) and ADPV, an analogue of ATP. On the basis of data analysis and energy metabolism, a plausible hypothesis “ATP dyssynthesis” is proposed here to elucidate the potential cytotoxicity mechanism of VO_2 nanomaterial through a vanadate-phosphate antagonism including two steps: (i) vanadate speciation from VO_2 surface chemistry; (ii) vanadate disturbing ATP synthesis as phosphate analogue. We give some feasible advice for compensating the potential cytotoxicity of VO_2 film from the perspective of surface coating and modification, and hope this work can stimulate wide scientific interest to search for more versatile material design strategies to balance the enhancement of energy-saving efficiency and the improvement of environmental safety of thermochromic VO_2 nanofilms for intelligent windows. This work is expected to provide new insights for VO_2-based versatile material design and practical applications.

Acknowledgements

The authors are grateful to the financial support by the high-tech project of MOST (2014AA032802) and the Science and Technology Commission of Shanghai Municipality (STCSM, No.: 14DZ2261203).

Notes and references

† Electronic Supplementary Information (ESI) available: Additional experimental details and relevant analysis. See DOI:
‡ These authors contributed equally to this work.

1. O. I. Asensio and M. A. Delmas, *Proceedings of the National Academy of Sciences*, 2015, **112**, E510-E515.
2. C. M. Lampert, *Materials Today*, 2004, **7**, 28-35.
3. R. Baetens, B. P. Jelle and A. Gustavsen, *Solar Energy Materials and Solar Cells*, 2010, **94**, 87-105.
4. W. Ning, H. Yizhong, S. Magdassi, D. Mandler, L. Hai and L. Yi, *RSC Advances*, 2013, **3**, 7124-7128.
5. N. Wang, S. Liu, X. T. Zeng, S. Magdassi and Y. Long, *Journal of Materials Chemistry C*, 2015, **3**, 6771-6777.
6. H. Zhou, J. Li, Y. Xin, X. Cao, S. Bao and P. Jin, *Journal of Materials Chemistry C*, 2015, **3**, 5089-5097.
7. A. Zylbersztejn and N. F. Mott, *Physical Review B*, 1975, **11**, 4383-4395.
8. Z. Zhang, Y. Gao, H. Luo, L. Kang, Z. Chen, J. Du, M. Kanehira, Y. Zhang and Z. L. Wang, *Energy & Environmental Science*, 2011, **4**, 4290-4297.
9. I. P. Parkin and T. D. Manning, *Journal of Chemical Education*, 2006, **83**, 393.
10. S. Sharifi, S. Behzadi, S. Laurent, M. Laird Forrest, P. Stroeve and M. Mahmoudi, *Chemical Society Reviews*, 2012, **41**, 2323-2343.
11. L. S. Rhoads, W. T. Silkworth, M. L. Roppolo and M. S. Whittingham, *Toxicology in Vitro*, 2010, **24**, 292-296.
12. X. Hu and Q. Zhou, *Chemical Reviews*, 2013, **113**, 3815-3835.
13. M. Song, S. Yuan, J. Yin, X. Wang, Z. Meng, H. Wang and G. Jiang, *Environmental Science & Technology*, 2012, **46**, 3457-3464.
14. N. B. Ress, B. J. Chou, R. A. Renne, J. A. Dill, R. A. Miller, J. H. Roycroft, J. R. Hailey, J. K. Haseman and J. R. Bucher, *Toxicological Sciences*, 2003, **74**, 287-296.
15. J. M. Wörle-Knirsch, K. Kern, C. Schleh, C. Adelhelm, C. Feldmann and H. F. Krug, *Environmental Science & Technology*, 2006, **41**, 331-336.
16. K. Kobayashi, S. Himeno, M. Satoh, J. Kuroda, N. Shibata, Y. Seko and T. Hasegawa, *Toxicology*, 2006, **228**, 162-170.
17. P. N. Saxena, A. Shukla, N. Saxena and J. Arya, *National Academy Science Letters*, 2010, **33(3-4)**, 95-101.
18. N. Fukuda and T. Yamase, *Biological & Pharmaceutical Bulletin*, 1997, **20**, 927-930.
19. S. Aendekerk, B. Ghysels, P. Cornelis and C. Baysse, *Microbiology*, 2002, **148**, 2371-2381.
20. S. Denayer, S. Matthijs and P. Cornelis, *FEMS Microbiology Letters*, 2006, **264**, 59-64.
21. J. M. Llobet and J. L. Domingo, *Toxicology Letters*, 1984, **23**, 227-231.
22. F. L. Assem and L. S. Levy, *Journal of Toxicology and Environmental Health, Part B*, 2009, **12**, 289-306.
23. D. Rehder, in *Interrelations between Essential Metal Ions and Human Diseases*, eds. A. Sigel, H. Sigel and R. K. O. Sigel, Springer Netherlands, 2013, pp. 139-169.

24. K. H. Thompson and C. Orvig, *Journal of Inorganic Biochemistry*, 2006, **100**, 1925-1935.
25. Y. Zhang, X.-D. Yang, K. Wang and D. C. Crans, *Journal of Inorganic Biochemistry*, 2006, **100**, 80-87.
26. L. S. Capella, M. R. Gefé, E. F. Silva, O. Affonso-Mitidieri, A. G. Lopes, V. M. Rumjanek and M. A. M. Capella, *Archives of Biochemistry and Biophysics*, 2002, **406**, 65-72.
27. J. O. M. Bockris and A. K. Reddy, *Modern electrochemistry: an introduction to an interdisciplinary area*, Springer Science & Business Media, 1973.
28. M. F. Toney, J. N. Howard, J. Richer, G. L. Borges, J. G. Gordon, O. R. Melroy, D. G. Wiesler, D. Yee and L. B. Sorensen, *Nature*, 1994, **368**, 444-446.
29. A. E. Russell, A. S. Lin and W. E. O'Grady, *Journal of the Chemical Society, Faraday Transactions*, 1993, **89**, 195-198.
30. K. F. Hayes, G. Redden, W. Ela and J. O. Leckie, *Journal of Colloid and Interface Science*, 1991, **142**, 448-469.
31. J. A. Davis, R. O. James and J. O. Leckie, *Journal of Colloid and Interface Science*, 1978, **63**, 480-499.
32. J. A. Yopps and D. W. Fuerstenau, *Journal of Colloid Science*, 1964, **19**, 61-71.
33. S. M. Ahmed, *Canadian Journal of Chemistry*, 1966, **44**, 1663-1670.
34. M. Aureliano, *Dalton Transactions*, 2009, 9093-9100.
35. N. D. Chasteen, *Vanadium in biological systems*, Springer, 1990.
36. S. Siekierski and J. Burgess, in *Concise Chemistry of the Elements*, ed. S. S. Burgess, Woodhead Publishing, 2002, pp. 131-154.
37. G. A. Parks, *Chemical Reviews*, 1965, **65**, 177-198.
38. M. Kosmulski, E. Mączka, W. Janusz and J. B. Rosenholm, *Journal of Colloid and Interface Science*, 2002, **250**, 99-103.
39. J. Li, G. Wang, D. Wang, Q. Wu, X. Jiang and X. Liu, *Journal of Colloid and Interface Science*, 2014, **436**, 160-170.
40. Y. Shen, W. Liu, K. Lin, H. Pan, B. W. Darvell, S. Peng, C. Wen, L. Deng, W. W. Lu and J. Chang, *Langmuir*, 2011, **27**, 2701-2708.
41. C. F. G. C. Geraldes and M. M. C. A. Castro, *Journal of Inorganic Biochemistry*, 1989, **35**, 79-93.
42. C. F. G. C. Geraldes and M. M. C.A. Castro, *Journal of Inorganic Biochemistry*, 1989, **37**, 213-232.
43. M. A. Habayeb and O. E. Hileman Jr, *Canadian Journal of Chemistry*, 1980, **58**, 2255-2261.
44. A. S. Tracey, M. J. Gresser and S. Liu, *Journal of the American Chemical Society*, 1988, **110**, 5869-5874.
45. A. S. Tracey, J. S. Jaswal, M. J. Gresser and D. Rehder, *Inorganic Chemistry*, 1990, **29**, 4283-4288.
46. G. C. Bond and S. Flamerz, *Applied Catalysis*, 1989, **46**, 89-102.
47. S. S. Soares, F. Henao, M. Aureliano and C. Gutiérrez-Merino, *Chemical Research in Toxicology*, 2008, **21**, 607-618.
48. B. Mukherjee, B. Patra, S. Mahapatra, P. Banerjee, A. Tiwari and M. Chatterjee, *Toxicology Letters*, 2004, **150**, 135-143.
49. M. Aureliano and R. M. C. Gândara, *Journal of Inorganic Biochemistry*, 2005, **99**, 979-985.
50. M. Valko, H. Morris and M. T. D. Cronin, *Current Medicinal Chemistry*, 2005, **12**, 1161-1208.
51. S. S. Soares, H. Martins, R. O. Duarte, J. J. G. Moura, J. Coucelo, C. Gutiérrez-Merino and M. Aureliano, *Journal of Inorganic Biochemistry*, 2007, **101**, 80-88.
52. S. S. Soares, C. Gutiérrez-Merino and M. Aureliano, *Aquatic Toxicology*, 2007, **83**, 1-9.
53. L. Cassimeris, V. R. Lingappa and G. Plopper, *Lewin's Cells*, Jones & Bartlett Publishers, Incorporated, 2010.
54. H. M. McBride, M. Neuspiel and S. Wasiak, *Current Biology*, 2006, **16**, R551-R560.
55. N. Dennis Chasteen, in *Copper, Molybdenum, and Vanadium in Biological Systems*, Springer Berlin Heidelberg, 1983, pp. 105-138.
56. M. Gresser and A. Tracey, in *Vanadium in Biological Systems*, ed. N. D. Chasteen, Springer Netherlands, 1990, pp. 63-79.
57. D. C. Crans, J. J. Smee, E. Gaidamauskas and L. Yang, *Chemical Reviews*, 2004, **104**, 849-902.
58. D. Rehder, *Angewandte Chemie International Edition in English*, 1991, **30**, 148-167.
59. D. C. Crans, C. M. Simone and J. S. Blanchard, *Journal of the American Chemical Society*, 1992, **114**, 4926-4928.
60. R. S. Ray, B. Rana, B. Swami, V. Venu and M. Chatterjee, *Chemico-Biological Interactions*, 2006, **163**, 239-247.
61. S. J. Stohs and D. Bagchi, *Free Radical Biology and Medicine*, 1995, **18**, 321-336.
62. G. S. Plumlee, S. A. Morman and T. L. Ziegler, *Reviews in Mineralogy and Geochemistry*, 2006, **64**, 5-57.
63. M. Valko, D. Leibfritz, J. Moncol, M. T. D. Cronin, M. Mazur and J. Telser, *The International Journal of Biochemistry & Cell Biology*, 2007, **39**, 44-84.
64. W. Dröge, *Physiological Reviews*, 2002, **82**, 47-95.
65. E. Burello and A. P. Worth, *Nanotoxicology*, 2011, **5**, 228-235.
66. Y. Xu and M. A. A. Schoonen, *American Mineralogist*, 2000, **85**, 543-556.
67. E. Burello and A. P. Worth, *Wiley Interdisciplinary Reviews: Nanomedicine and Nanobiotechnology*, 2011, **3**, 298-306.
68. M. J. Gresser, A. S. Tracey and K. M. Parkinson, *Journal of the American Chemical Society*, 1986, **108**, 6229-6234.

The potential cytotoxicity of thermochromic VO_2 nanofilm to human cells presumably originates from the ATP dyssynthesis by vanadate-phosphate antagonism.

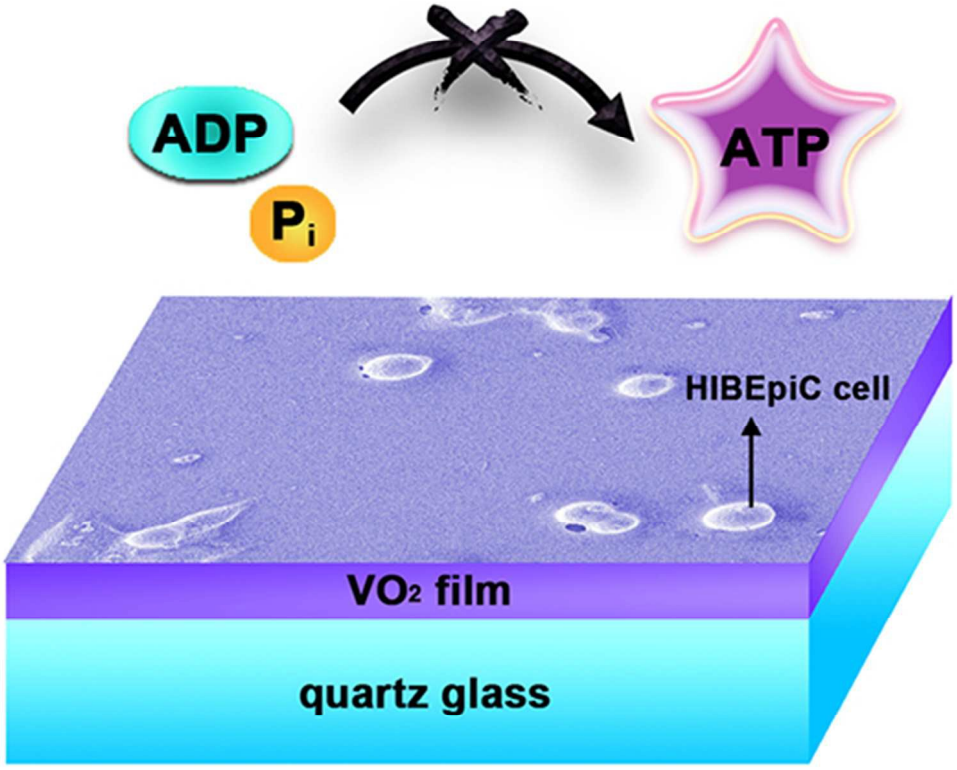

46x39mm (300 x 300 DPI)